IEEE Photonics Journal
An IEEE Photonics Society Publication

Open Access

Polarization Coupling of X-Cut Thin Film Lithium Niobate Based Waveguides

Volume 12, Number 3, June 2020

Jingyi Wang
Pengxin Chen
Daoxin Dai
Liu Liu

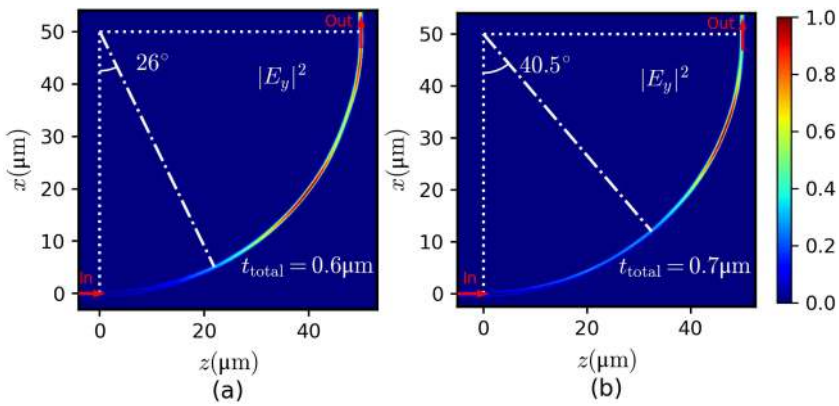

DOI: 10.1109/JPHOT.2020.2995317

Polarization Coupling of *X*-Cut Thin Film Lithium Niobate Based Waveguides

Jingyi Wang [1], **Pengxin Chen** [1], **Daoxin Dai** [2], **and Liu Liu** [2]

[1]Centre for Optical and Electromagnetic Research, Guangdong Provincial Key Laboratory of Optical Information Materials and Technology, South China Academy of Advanced Optoelectronics, South China Normal University, Higher-Education Mega-Center, Guangzhou 510006, China
[2]State Key Laboratory for Modern Optical Instrumentation, Centre for Optical and Electromagnetic Research, Zhejiang Provincial Key Laboratory for Sensing Technologies, Zhejiang University, Hangzhou 310058, China

DOI:10.1109/JPHOT.2020.2995317
This work is licensed under a Creative Commons Attribution 4.0 License. For more information, see https://creativecommons.org/licenses/by/4.0/

Manuscript received February 7, 2020; revised April 28, 2020; accepted May 11, 2020. Date of publication May 18, 2020; date of current version June 22, 2020. This work was supported in part by the National Major Research and Development Program (2019YFB1803902), in part by the National Nature Science Foundation of China (61675069), in part by the Guangzhou Science and Technology Program (201707010444), and in part by the Special Funds for the Cultivation of Guangdong College Students' Scientific and Technological Innovation ("Climbing Program"). Corresponding authors: Pengxin Chen and Liu Liu (e-mail: chenpx@m.scnu.edu.cn; liuliuopt@zju.edu.cn).

Abstract: Thin film lithium niobate (LN) shows great potentials for highly compact passive and active devices. As LN is an anisotropic material, waveguides made on it exhibit different mode properties from those on conventional isotropic materials. We study the effective refractive indices of fundamental modes of two polarizations in etched ridge waveguides on an *X*-cut LN thin film. Mode hybridization phenomenon, where the effective refractive indices of the two polarizations are close, is analyzed in detail with different structural parameters. Transmission through a 90° bend, which is a typical routing element for a photonic chip, is simulated. Significant polarization coupling related to the mode evaluation through the bend is observed, and becomes the dominant fact limiting the performance of this element. In order to ensure a low bending loss, the required bending radius is much larger than that for waveguides on an in-plane isotropic material, e.g. a *Z*-cut LN thin film. Mode hybridization also plays an important role in the performance of the 90° bend, which should be avoided. Generally, decreasing the thickness of the LN thin film, working at a longer wavelength, or confining the propagation angle on a chip would help to decrease the polarization coupling.

Index Terms: Ridge waveguide, lithium niobate, polarization coupling.

1. Introduction

In the past few decades, integrated photonics has developed rapidly and there exist many different materials, such as SiO_2 [1], [2], Si_3N_4 [3], silicon on insulator (SOI) [4], [5], III-IV compound semiconductors [6], and lithium niobate (LN) [7], to fabricate different functional photonic elements. Among them, LN has excellent material properties, including large Pockels effect, acousto-optic effect, nonlinear coefficient, as well as a wide transparent wavelength band from ultraviolet (UV) to mid-infrared (IR), which make LN an attractive platform for active and passive devices [8]–[11], such as high-speed optical modulators. Traditional LN modulators are based on low index contrast waveguide realized through proton exchange or Ti diffusion technologies on a bulk LN substrate, where the diffused waveguides have a low confinement for optical fields and the footprint of a modulator is

relatively large. Therefore, this kind of waveguide structure is not suitable for high-density photonic integration [8], [12], [13]. Recently, the development of crystal ion-slicing technology makes it possible to produce thin-film LN on insulator (LNOI) wafers with a buried silicon oxide buffer layer [13]. Benefited from the large refractive index contrast between the LN and the silicon oxide, as well as the robust dry-etching technology of LN, ridge waveguides fabricated on thin-film LN present a tight light confinement, and a small bending radius can also be expected. High-performance and highly-integrated electro-optic modulators [9], [14], [15], micro-ring resonators [16]–[18], grating couplers [19], and photonic crystal devices [20], [21] fabricated on the thin film LN have been demonstrated on this LNOI platform.

Usually, many integrated optical elements are polarization-dependent and their response changes as a function of the polarization state in the waveguides. In order to have a given response, the polarization state of the mode in an integrated waveguide is maintained as quasi-transverse-electrical (quasi-TE) or quasi-transverse-magnetic (quasi-TM) [22]. Generally, for integrated circuits based on an isotropic material, the coupling between the two polarized modes is very weak in routing waveguides on a chip, such as straight waveguides, bending waveguides, etc., and can usually be ignored, unless special designs are adopted to enhance the polarization coupling to build devices like polarization splitters or polarization rotators [23]. Unfortunately, for anisotropic materials, such as LN, because of the strong material birefringence, the coupling between the two polarized modes cannot be ignored anymore. The propagation direction of the waveguide on a chip can largely affect the mode properties [24]. This effect is further enhanced for a high refractive index contrast waveguide based on LNOI [10], [11]. In this paper, we analyze the effective refractive index of the fundamental quasi-TE and quasi-TM modes and their difference in a ridge waveguide made on an X-cut thin LN film. The dependence of the mode hybridization effect on structural parameters of the waveguide is investigated in detail. The total transmission and the polarization coupling through a 90° bend is studied, whose results comply with the mode properties analyses. Guidelines for designing an LNOI waveguide structure suitable for on chip routing is also discussed.

2. Mode Property

The ridge straight waveguide structure analyzed here is shown in Fig. 1(a), which is fabricated on a X-cut LN thin film on a silicon oxide substrate, the cladding material is also assumed to be silicon oxide. In Fig. 1(a), the upper-case XYZ represents the coordinate system of the LN crystal while the lower-case xyz represents the coordinate system of the waveguide. Fig. 1(b) shows the refractive index ellipse of the LN material. The angle between the axis z (the propagation direction of the ridge waveguide) and the optical axis Y of the LN material is ϕ. When $\phi = 0^\circ$, the ridge waveguide is perpendicular to the optical axis Z of the LN material, which means it is a X-cut and Y-propagation waveguide structure as shown in Fig. 1(c). In this case, the quasi-TM mode mainly sees the ordinary refractive index n_o of the LN material, while the quasi-TE mode mainly sees the extraordinary refractive index n_e. When the angle ϕ is 90°, the ridge waveguide is then X-cut and Z-propagation. In this case, the quasi-TE and the quasi-TM modes both see the ordinary refractive index n_o. With the variation of the angle ϕ from 0° to 90° such as in a 90° bend, the quasi-TM mode always sees the same refractive index n_o, while the quasi-TE mode experiences a large refractive index change from n_e to n_o, which would cause an abnormal polarization coupling as to be discussed below. On the other hand, for a ridge waveguide on a Z-cut LNOI substrate either the quasi-TE or the quasi-TM modes keep seeing the same index (n_o for the quasi-TE mode and n_e for the quasi-TM mode) whatever the propagation direction of the waveguide is. This is similar to the case of a waveguide built on an isotropic material.

Fig. 1(d) shows effective refractive indices $n_{\text{eff,TE}}$ and $n_{\text{eff,TM}}$ of the quasi-TE and the quasi-TM modes at 1.31 μm and 1.55 μm wavelength when the propagation angle ϕ of the straight waveguide varies from 0° to 90°. Other structural parameters are the total thickness of the LN film $t_{\text{total}} = 0.6$ μm, the normalized etching thickness (defined as the ratio of the slab thickness on the total LN film thickness) $r_{\text{slab}} = 0.5$, the width of the ridge (defined at the center of the ridge) $w = 1.0$ μm, the sidewall angle $\theta_{\text{etch}} = 60^\circ$, and silicon oxide is considered as the cladding. These are typical

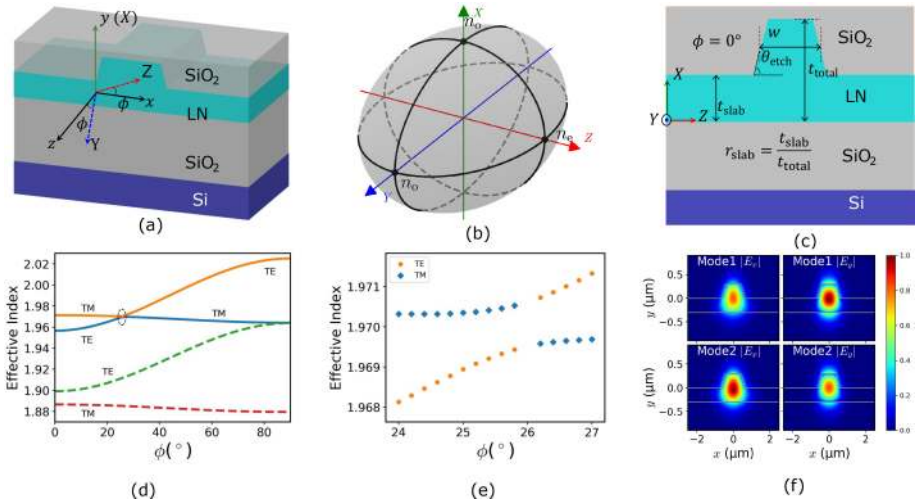

Fig. 1. (a) Coordinate systems of the LN ridge waveguide and the LN crystal. (b) Refractive index ellipse of the LN material. (c) Cross section of the LN ridge waveguide when the propagation angle ϕ is 0°. (d) Effective refractive indices of the quasi-TE and the quasi-TM modes for different ϕ, the wavelengths of the solid curves are 1.31 μm and the dashed curves are 1.55 μm. (e) Zoom-in view of the area labeled by the dashed ellipse in (d). (f) Mode profiles for the two fundamental modes when the angle ϕ is 26° at 1.31 μm wavelength.

values for thin film LN waveguides used for high-speed electro-optical (EO) modulators [9]. As expected, the effective refractive indices of the quasi-TE mode show a large variation at different ϕ, while those of the quasi-TM mode are relatively insensitive to ϕ. At $\phi = 90^\circ$ (where the quasi-TE and quasi-TM modes both see n_o), the effective refractive index of the quasi-TE mode is higher than that of the quasi-TM mode for both wavelengths. This relation is held normally for a ridge waveguide on an isotropic material [25]. However, at $\phi = 0^\circ$ and 1.31 μm wavelength, the effective refractive index of the quasi-TE mode becomes less than that of the quasi-TM mode. There exists a "crossing" point ($\phi = 26^\circ$) for the curves of the two polarizations at 1.31 μm wavelength as shown in Fig. 1(d). Due to the anisotropy of the LN material, the symmetry of waveguide structure is broken even in a straight waveguide which leads to the mode hybridization at this point, and this "crossing" would actually be an anti-crossing as shown in Fig. 1(e). This mode hybridization phenomenon is further explained through the mode field distributions in Fig. 1(f). One can see that the optical fields of the two modes have a large portion in both E_x and E_y components. When the waveguide structure goes through this point, e.g., in a 90° bend, the mode hybridization would result in a significant, and usually unwanted, the coupling between the two polarized modes. It is worthwhile to note that this phenomenon would not exist for waveguides on an isotropic material or a Z-cut LN thin film, where the refractive index is isotropic in any in-plane direction. Therefore, in order to investigate this inter-polarization coupling on an X-cut LNOI wafer, it is necessary to study the effective refractive indices of the two fundamental modes and their difference, defined as $\Delta n_{\mathrm{TE-TM}} = n_{\mathrm{eff,TE}} - n_{\mathrm{eff,TM}}$, with respect to the structural parameters of the waveguide.

Fig. 2(a) shows the difference $\Delta n_{\mathrm{TE-TM}}$ as a function of the wavelength and the ridge width w at $t_{\mathrm{total}} = 0.6$ μm, $r_{\mathrm{slab}} = 0.5$, $\theta_{\mathrm{etch}} = 60^\circ$ when $\phi = 0^\circ$. It is obvious that $\Delta n_{\mathrm{TE-TM}}$ is not sensitive to w, as long as the width w is wider than 1.0 μm in this case. On the other hand, the working wavelength poses a significant influence on $\Delta n_{\mathrm{TE-TM}}$. $\Delta n_{\mathrm{TE-TM}}$ almost demonstrates a linear increase with respect to the increase of the wavelength. The black solid line in Fig. 2(a) indicates the contour line where $|\Delta n_{\mathrm{TE-TM}}|$ is at its minimum (hereafter, denoted as $\Delta n_{\mathrm{TE-TM}} \approx 0$). This contour line divides the results shown in Fig. 2(a) into two regions, i.e., the "red" region, where $\Delta n_{\mathrm{TE-TM}} > 0$ and the wavelength is longer, and the "blue" region, where $\Delta n_{\mathrm{TE-TM}} < 0$ and the wavelength is shorter. Since $\Delta n_{\mathrm{TE-TM}}$ increases as the propagation angle ϕ gets larger as shown in Fig. 1(d),

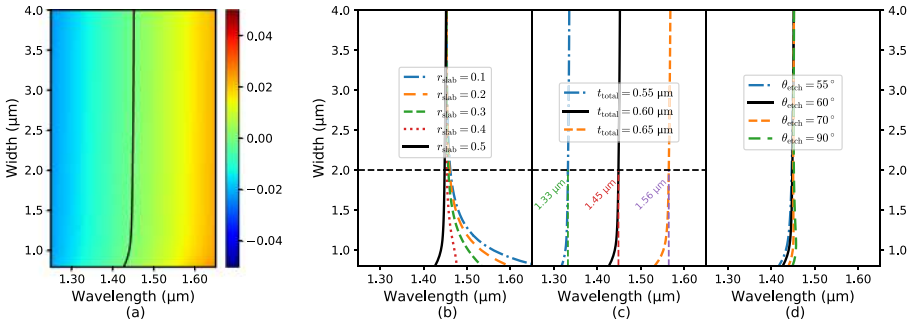

Fig. 2. (a) Difference Δn_{TE-TM} between the effective refractive indices of the quasi-TE and the quasi-TM modes when the width w varies from 0.8 μm to 4.0 μm for $t_{total} = 0.6$ μm, $r_{slab} = 0.5$, $\theta_{etch} = 60°$. The black curve dictates $\Delta n_{TE-TM} \approx 0$. (b)–(d) Contour curves of $\Delta n_{TE-TM} \approx 0$ for different structural parameters.

the "red" region of Fig. 2(a) would ensure that the effective refractive index of the quasi-TE mode is always larger than that of the quasi-TM mode, i.e., no mode hybridization would occur, at any in-plane propagation directions. On the contrary, the mode hybridization would happen at a certain propagation angle ϕ in the "blue" region of Fig. 2(a). Based on these analyses, the contour line of $\Delta n_{TE-TM} \approx 0$ (hereafter, referred as the mode hybridization boundary) is of great importance to discuss the polarization coupling during a 90° bend. Fig. 2(b)–(d) plot the contour curves of $\Delta n_{TE-TM} \approx 0$ for different normalized etching thicknesses r_{slab}, total film thicknesses t_{total}, and sidewall angles θ_{etch}. The rest parameters are kept the same as those in Fig. 2(a). From Fig. 2(b), one can find that the mode hybridization boundaries moves towards longer wavelengths if r_{slab} decreases. Note that this effect is only obvious if the ridge width w is narrower than 2.0 μm. Beyond this point, the influence of r_{slab} becomes insignificant. On the other hand, the total film thickness t_{total}, as shown in Fig. 2(c), does pose a significant impact on the mode hybridization boundary. The contour curve of $\Delta n_{TE-TM} \approx 0$ moves to longer wavelengths for about 0.11 μm as t_{total} increases for only 50 nm. From this analysis, one can conclude that a thinner LN film is more preferable for devices working for a shorter wavelength. For example, in order for the structure working for both C and O bands, t_{total} is better kept less than 0.5 μm to avoid mode hybridization in a 90° bend. On the other hand, one would like to choose a thick film for, e.g., an EO or nonlinear device, since in this case the mode confinement in the LN material is higher. Therefore, a compromise for choosing t_{total} has to be agreed between maximizing the optical interaction with the LN material and a complex routing on the LNOI wafer for practical applications. Obviously, the thickness uniformity of the LN film across the whole LNOI wafer becomes also one important figure to consider.

For the sidewall angle θ_{etch}, its influence on the mode hybridization boundary is however insignificant whatever w is, as shown in Fig. 2(d). The curves here are almost overlapped. The influence of θ_{etch} is further studied in Fig. 3, where almost vertical straight lines for $\Delta n_{TE-TM} \approx 0$ curves can be observed, except that for w and r_{slab} are both small as showed in Fig. 3(a). This means that the mode hybridization boundary is also not sensitive to θ_{etch} in most cases. Although a non-vertical etching sidewall could induce an increased polarization coupling for a 90° bend in some waveguide structure, e.g., an SOI wire waveguide when the bending radius is very small [26], such an effect would not be dominant in the present structure as to be discussed in the next section.

In above analyses, we assumed an arbitrary routing on an LN thin film, i.e., ϕ from 0° to 90°. However, in some applications, such as an S-bend structure, a 90° bend is unnecessary. It is therefore meaningful to study the propagation angle dependence of Δn_{TE-TM} in detail. Fig. 4(a) plots the effective refractive index difference Δn_{TE-TM} as a function of wavelength and the propagation angle ϕ for $w = 1.0$ μm, $r_{slab} = 0.5$, $t_{total} = 0.6$ μm and $\theta_{etch} = 60°$. The solid contour curve is for $\Delta n_{TE-TM} \approx 0$, i.e., the mode hybridization boundary, which also divides the plot into "red" and "blue" regions, similar to those in Fig. 2(a). When the wavelength is at 1.31 μm, Δn_{TE-TM} varies from -0.0145 to 0.062, across the "blue" and the "red" regions, while for 1.55 μm, Δn_{TE-TM} varies

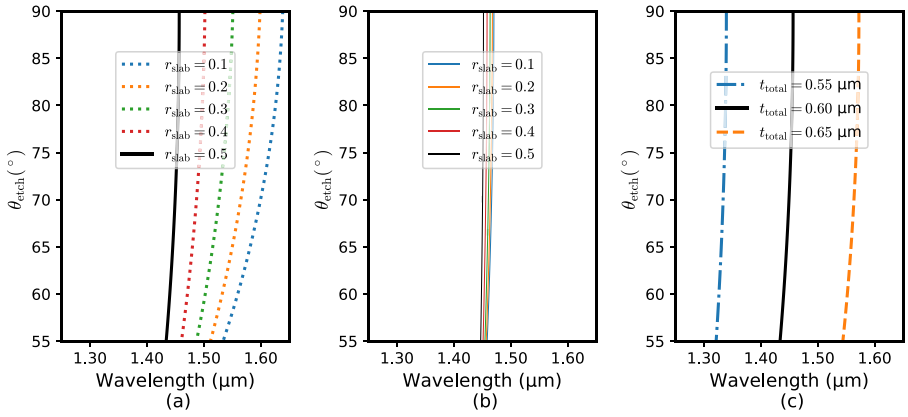

Fig. 3. Contour curves of $\Delta n_{TE-TM} \approx 0$ as a function of the wavelength and the waveguide sidewall angle θ_{etch} for different normalized etching thicknesses r_{slab} at (a) $w = 1.0$ μm and (b) $w = 2.0$ μm, and (c) for different total film thicknesses t_{total} at $w = 1.0$ μm. The other structural parameters are the same in Fig. 2(a).

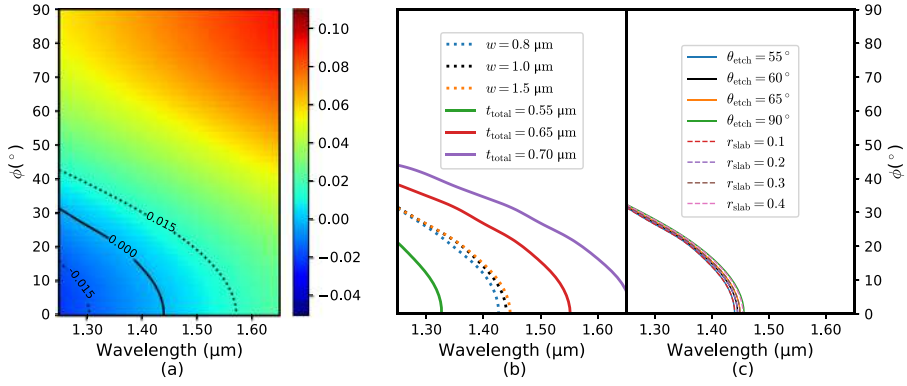

Fig. 4. (a) Difference Δn_{TE-TM} when ϕ varies from 0° to 90° for $w = 1.0$ μm, $t_{total} = 0.6$ μm, $r_{slab} = 0.5$ and $\theta_{etch} = 60°$. The solid contour curve is at $\Delta n_{TE-TM} \approx 0$. (b) Contour curves of $\Delta n_{TE-TM} \approx 0$. Dashed curves are for different ridge widths w with $t_{total} = 0.6$ μm. Solid curves are for different total LN film thicknesses t_{total} with $w = 1.0$ μm. (c) Contour curves of $\Delta n_{TE-TM} \approx 0$. Dashed curves are for different normalized etching thicknesses r_{slab} with $\theta_{etch} = 60°$. Solid contour curves are for different sidewall angles θ_{etch} with $r_{slab} = 0.5$.

from 0.013 to 0.084 and stays in the "red" region. This result can also be drawn from Fig. 1(d). Actually, for wavelengths longer than 1.44 μm, Δn_{TE-TM} is always larger than zero regardless of ϕ. This implies that at these wavelengths a waveguide with the present structure could be routed in any direction on a LNOI wafer without mode hybridization. For wavelengths smaller than 1.44 μm the mode hybridization can be avoided, if the propagation angle ϕ of the waveguide is confined in either the "red" or the "blue" region without going across them. This provides a guideline of choosing waveguide routing angles when designing the mask layout. Fig. 4(b) also shows the contour curves of $\Delta n_{TE-TM} \approx 0$ for different waveguide widths w (dotted curves) and total thicknesses t_{total} (solid curves), and Fig. 4(c) shows that for different normalized etching thicknesses r_{slab}. Its obvious that the mode hybridization boundary moves to longer wavelengths as t_{total} increases. The influence of the other three parameters is relatively small.

Another structural parameter which could influence the mode hybridization issue is the refractive index n_c of the cladding material. In above analyses, silicon oxide cladding is always assumed. Fig. 5(a) shows the mapping of Δn_{TE-TM} with different n_c from 1.0 (air) to 1.6 (polymer) at different wavelengths for $w = 1.0$ μm, $r_{slab} = 0.5$, $t_{total} = 0.6$ μm and $\theta_{etch} = 60°$. It can be found that the

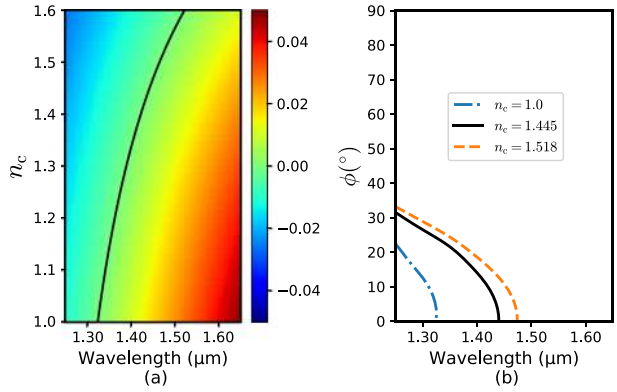

Fig. 5. (a) Difference $\Delta n_{\mathrm{TE-TM}}$ when the index of cladding n_c varies from 1.0 to 1.6 for $w = 1.0$ μm, $t_{\mathrm{total}} = 0.6$ μm, $r_{\mathrm{slab}} = 0.5$, $\theta_{\mathrm{etch}} = 60^{\circ}$. The black curve is at $\Delta n_{\mathrm{TE-TM}} \approx 0$. (b) Contour curves of $\Delta n_{\mathrm{TE-TM}} \approx 0$ as a function of wavelength and the propagation angle ϕ at different cladding index n_c.

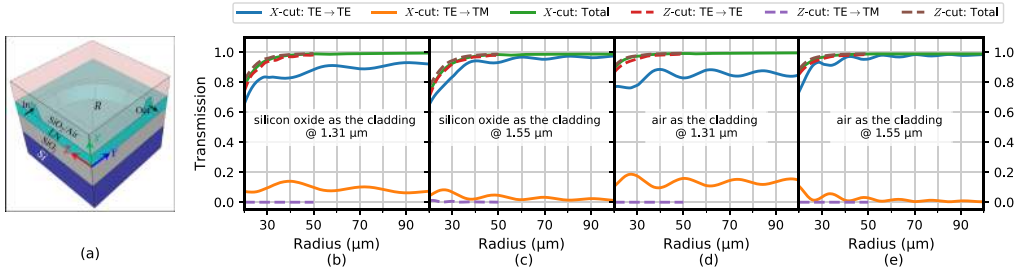

Fig. 6. (a) Schematic of a 90° bend with the ridge waveguide on an X-cut LN thin film. (b)–(e) Transmission through the 90° bend at different bending radius. Solid curves are for structures on an X-cut LN thin film and dotted curves are for structures on a Z-cut LN thin film. In (b) & (c) the cladding material is silicon oxide, and in (d) & (e) the cladding material is air. Simulation parameters: $t_{\mathrm{total}} = 0.60$ μm, $r_{\mathrm{slab}} = 0.5$, $w = 1.0$ μm, $\theta_{\mathrm{etch}} = 60^{\circ}$, and the wavelength is 1.31 μm for (b) & (d) and 1.55 μm for (c) & (e).

contour curve of $\Delta n_{\mathrm{TE-TM}} \approx 0$ exhibits a monotonous increase with a rate of ˜330 nm/RIU (RIU: refractive index unit). This trend is further explained in Fig. 5(b), where the mode hybridization boundary moves towards the left-bottom corner of the plot when decreasing the cladding refractive index. This means that the "red" region, i.e., $\Delta n_{\mathrm{TE-TM}} > 0$, is expanded through using a lower refractive index material, such as air instead of silicon oxide, as the cladding. This is one strategy to avoid mode hybridization for the present waveguide structure.

3. Bending Performance

In the previous section, the mode properties of different waveguide structures on an X-cut LN thin film have been mainly discussed, which provides qualitative guidelines to avoid mode hybridization. Here, the realistic polarization coupling performance during a 90° bend is further studied using three-dimensional finite-difference time-domain simulations. The simulation model is sketched in Fig. 6(a). A quarter of a ring is used as the bending section, where two straight waveguides are connected as the input and output ports. A quasi-TE mode field is employed as the input, and the input waveguide is along the Y direction of the LN material. This is the most common waveguide direction for EO or nonlinear devices on an X-cut LN thin film, where the majority of the electrical field can interact with the desired optical axis of the LN material. After transmitting through the 90° bend, the power carried in the quasi-TE and quasi-TM modes at the output port is then analyzed.

Fig. 6(b) plots the transmission coefficient of the structure at 1.31 μm wavelength. The transmission of TE→TE (TM) is defined as the ratio between the power of the quasi-TE (quasi-TM)

at the output and that of the input quasi-TE mode. The total transmission is the sum of TE→TE and TE→TM transmission. One can find that the transmission for the quasi-TE mode experiences a high loss even when the bending radius is relatively large. A large portion of power, higher than 5%, is coupled to the quasi-TM mode. This large polarization coupling is expected from the discussions in the previous section, since for 1.31 μm wavelength the mode hybridization happens during a 90° bend. As a comparison, the same waveguide structure on a *Z*-cut LN thin film is also studied, where, as we mentioned before, no mode hybridization would exist in this type of structure. Although the quasi-TE mode transmission also exhibits a high loss if the bending radius is small, for bending radii larger than 50 μm the transmission is close to 1. The polarization coupling is always small, less than 0.03%. It is also worth to mention that the total transmission curves for both *X*-cut and *Z*-cut LN thin film are similar. From this analysis, we can conclude that the large polarization coupling for the *X*-cut LN thin film mainly results from the anisotropy of the material and the corresponding mode hybridization. For 1.55 μm wavelength, the transmission of the same structure is shown in Fig. 6(c). One can find that the polarization coupling at this longer wavelength is much smaller than that at 1.31 μm wavelength. This complies with the discussion in the previous section, since in this case mode hybridization would not happen during a 90° bend. However, as compared to the case of the *Z*-cut LN thin film, the polarization coupling is still relatively high. In an in-plane isotropic material, the polarization coupling, as well as the total bending loss, from a 90° bend mainly comes from the mode mismatch at the junction of the straight and the bending waveguide sections [27]. The bending section itself, in this case, can be considered as a straight waveguide in a cylindrical coordinate system, and as a result there would be no mode coupling. Although the bending section would also result in a radiation loss, it, as compared to the mode mismatching loss, is insignificant in a high index contrast system for large bending radii [28]. However, in an anisotropic material, such as the *X*-cut LN thin film, there exists an extra source for the polarization coupling. The bending section can no longer be considered as an invariant straight waveguide even in a cylindrical coordinate system, as the optical mode sees a core material with variant refractive indices along the bend. As demonstrated in Fig. 1(d), the effective refractive index of the quasi-TE mode is continuously changing along the bend. This situation is similar to a tapered structure [29]. To ensure a low transmission loss for such a *Z*-variant structure, the adiabatic criterion should be applied [30], which requires that the variation should be "slow" enough or the device long enough. In the bending structure discussed here, this means the bending radius should be sufficiently large. This is obvious, in Fig. 6(c), that the general trend of the polarization coupling, although some ripples presents, decreases as increasing the bending radius towards 100 μm. However, this approach can only be applied for the case with no mode hybridization. If mode hybridization does happen, e.g., at 1.31 μm wavelength, increasing the bending radius would not help reduce the coupling to another polarization, since the adiabatic criterion only ensures that the optical field would follow one mode along the *Z*-variant structure [30]. At the mode hybridization point in the current structure, an anti-crossing for the modes presents as discussed in Fig. 1(e). The polarization coupling would actually be enhanced if the bending radius is large. This effect can also be observed in Fig. 6(b) and 6(d), where the cladding material is silicon oxide and air, respectively, at 1.31 μm wavelength. For these two cases, the mode hybridization both exist through the bend as show in Fig. 5(a). Increasing the bending radius up to 100 μm does not shows an obvious suppression for the polarization coupling. Theoretically, further increasing the bending radius would result in a total transform of the quasi-TE mode to the quasi-TM mode, i.e., a polarization rotator. Although being useful, the optimization of such a device is out of the scope of this paper. In order to decrease the polarization coupling, one should work further away from the mode hybridization boundary. The adiabatic criterion also suggests that the variation rate of the structure is proportional to the effective refractive index difference of adjacent modes [25]. Increasing the difference of the effective refractive indices of the quasi-TE and the quasi-TM modes would help to decrease the polarization coupling. According to Fig. 5(b), decreasing the refractive index of the cladding material helps move the mode hybridization boundary towards short wavelength, and hence, increase the effective refractive index difference of the two modes at 1.55 μm. This is confirmed in Fig. 6(e) where the cladding material is changed from silicon oxide to air, where the polarization coupling is

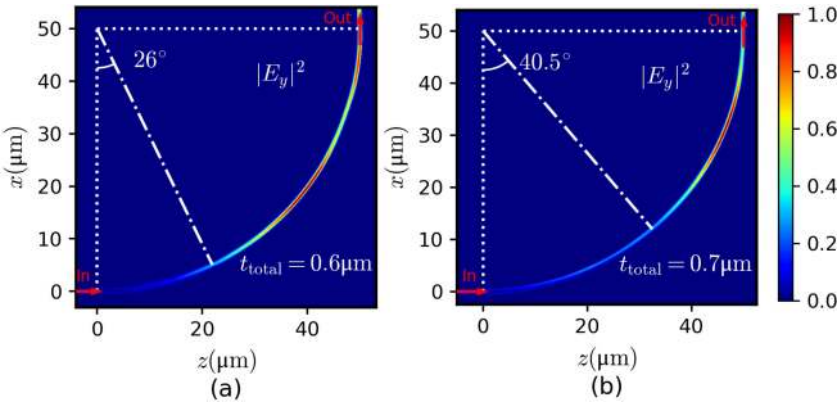

Fig. 7. The normalized $|E_y|^2$ profile of the 90° bend with 50 μm bending radius for (a) $t_{\text{total}} = 0.6$ μm and (b) $t_{\text{total}} = 0.7$ μm. The wavelength is at 1.31 μm. The other structural parameters are the same in Fig. 6(b).

obviously reduced. It can be less than 0.9% for bending radii larger than 90 μm. The transmission for the quasi-TE mode is also better than 97.8% in these cases.

To further study the polarization coupling effect, the $|E_y|^2$ field distributions through the 90° bend at 1.31 μm wavelength is shown in Fig. 7(a) and (b), when the bending radius is 50 μm and the total film thickness is 0.6 μm and 0.7 μm, respectively. The rest of the parameters is the same as those in Fig. 6(b). The input light is the quasi-TE polarized, and therefore, the E_y field, i.e., the minor component of the E field, is small at the input port. At the output port, the E_y field increases, which means a significant polarization coupling occurs in both cases. This is not surprising, since the mode hybridization does happen at $\phi = 26^\circ$ and $\phi = 40.5^\circ$, respectively, for these two cases as presented in Fig. 4(b). These two angles are also marked in Fig. 7. One can find that the polarization coupling only becomes severe around the mode hybridization boundaries. The analyses here also prove one conclusion drawn in the previous section, i.e., if the mode hybridization cannot be avoided in a 90° bend in some circumstances, one solution is to confine the propagation angle ϕ on a chip. The polarization coupling can be effectively reduced, if the routing angle is kept within 26° and 40.5°, respectively, for these two cases.

4. Discussion and Conclusion

LN is an important material for integrated photonics, especially for high-performance modulators and nonlinear devices. Due to its anisotropy, the effective refractive indices of the quasi-TE and the quasi-TM modes for a planar waveguide on an LN thin film exhibit very different properties from that on an isotropic material. In this paper, the effective refractive index difference $\Delta n_{\text{TE-TM}}$ of these two fundamental modes has been analyzed in detail in an etched ridge waveguide built on an X-cut LNOI wafer along different in-plane propagation angle ϕ. In some cases, mode hybridization would happen, which would induce a severe and unwanted polarization coupling when routing the waveguide arbitrarily in plane, e.g., a 90° bend. From the mode property simulations, one can find that the total thickness of the LN film is the major factor for affecting the mode hybridization. In this sense, it is better to use a thinner LN film for a device, especially when working at a shorter wavelength. However, decreasing the LN film thickness would decrease the mode confinement in the LN material, and hence decrease the EO or nonlinear interaction. A compromise has to be agreed when designing the LNOI wafer structure. Besides, using a low refractive index material, such as air, as the cladding can also help to avoid the mode hybridization.

The bending loss and the polarization coupling in a 90° bend has also been studied. On an X-cut LNOI wafer, the bending losses through a 90° bend is much higher than those from the same waveguide structure on a Z-cut LNOI wafer. The bending performance in this case is no longer

limited by the radiation loss of the bending waveguide and the mode transition loss between it and the input/output straight waveguide, which are commonly main sources for bending losses for a high refractive index contrast waveguide system on an isotropic material, such as silicon or silicon nitride [4], as well as a *Z*-cut LN thin film. The mode continuously evolves in the bending section, and a nonnegligible coupling between the quasi-TE and the quasi-TM modes can happen. When designing a waveguide layout, one has to choose a relatively large bending radius, times larger than what is needed on an in-plane isotropic material, to avoid a significant polarization coupling. If mode hybridization would happen during the 90° bend, increasing the bending radius would not help on reducing the polarization coupling. To solve this problem, redesigning the waveguide structure according to the mode properties analyzed here would be necessary. Otherwise, one has to confine the propagation angle on a chip to reduce the polarization coupling.

Conventional diffusion based waveguides on bulk LN substrate also presents such a mode hybridization phenomenon shown here [22]. However, in normal devices on a bulk LN substrate, e.g., an EO modulator or a nonlinear waveguide, the mode hybridization and the related polarization coupling is somehow not an issue since the bend radius is large, in the order of centimeter, to reduce the radiation loss. In the high refractive index contrast waveguides on the LNOI substrate, the influence of the pure bending related losses becomes insignificant, as discussed above, as compared to the mode evolution related coupling, which now becomes the limiting fact for the routing of such a waveguide.

References

[1] C. R. Doerr and K. Okamoto, "Advances in silica planar lightwave circuits," *J. Lightw. Technol.*, vol. 24, no. 12, pp. 4763–4789, Dec. 2006.

[2] T. Miya, "Silica-based planar lightwave circuits: Passive and thermally active devices," *IEEE J. Sel. Topics Quantum Electron.*, vol. 6, no. 1, pp. 38–45, Jan. 2000.

[3] C. G. H. Roeloffzen *et al.*, "Low-loss Si_3N_4 triplex optical waveguides: Technology and applications overview," *IEEE J. Sel. Topics Quantum Electron.*, vol. 24, no. 4, pp. 1–21, Jul. 2018.

[4] D. Dai, "Advanced passive silicon photonic devices with asymmetric waveguide structures," *Proc. IEEE*, vol. 106, no. 12, pp. 2117–2143, Dec. 2018.

[5] D. Thomson *et al.*, "Roadmap on silicon photonics," *J. Opt.*, vol. 18, no. 7, Jun. 2016, Art. no. 073003.

[6] G. Duan *et al.*, "Hybrid III–V on Silicon Lasers for Photonic Integrated Circuits on Silicon," in *IEEE J. Sel. Topics Quantum Electron.*, vol. 20, no. 4, pp. 158–170, Jul./Aug. 2014, Art. no. 6100213, doi: 10.1109/JSTQE.2013.2296752.

[7] C. Bulmer and W. Burns, "Polarization characteristics of $LiNbO_3$ channel waveguide directional couplers," *J. Lightw. Technol.*, vol. 1, no. 1, pp. 227–236, Mar. 1983.

[8] E. Saitoh, Y. Kawaguchi, K. Saitoh, and M. Koshiba, "A design method of lithium niobate on insulator ridge waveguides without leakage loss," *Opt. Express*, vol. 19, no. 17, pp. 15 833–15 842, Aug. 2011.

[9] M. He *et al.*, "High-performance hybrid silicon and lithium niobate Mach-Zehnder modulators for 100 Gbit s^{-1} and beyond," *Nature Photon.*, vol. 13, no. 5, pp. 359–364, May 2019.

[10] A. Pan, C. Hu, C. Zeng, and J. Xia, "Fundamental mode hybridization in a thin film lithium niobate ridge waveguide," *Opt. Express*, vol. 27, no. 24, pp. 35 659–35 669, Nov. 2019.

[11] A. Kaushalram, S. A. Samad, G. Hegde, and S. Talabattula, "Tunable large dispersion in hybrid modes of lithium niobate-on-insulator multimode waveguides," *IEEE Photon. J.*, vol. 11, no. 3, Jun. 2019, Art. no. 6601908.

[12] O. Stepanenko, E. Quillier, H. Tronche, P. Baldi, and M. De Micheli, "Highly confining proton exchanged waveguides on *Z*-cut $LiNbO_3$ with preserved nonlinear coefficient," *IEEE Photon. Technol. Lett.*, vol. 26, pp. 1557–1560, Aug. 2014.

[13] A. Rao and S. Fathpour, "Compact lithium niobate electrooptic modulators," *IEEE J. Sel. Topics Quantum Electron.*, vol. 24, no. 4, pp. 1–14, Jul. 2018.

[14] M. Jin, J.-Y. Chen, Y. M. Sua, and Y.-P. Huang, "High-extinction electro-optic modulation on lithium niobate thin film," *Opt. Lett.*, vol. 44, no. 5, pp. 1265–1268, Mar. 2019.

[15] C. Wang, M. Zhang, B. Stern, M. Lipson, and M. Lončar, "Nanophotonic lithium niobate electro-optic modulators," *Opt. Express*, vol. 26, no. 2, pp. 1547–1555, Jan. 2018.

[16] B. Desiatov, A. Shams-Ansari, M. Zhang, C. Wang, and M. Lončar, "Ultra-low-loss integrated visible photonics using thin-film lithium niobate," *Optica*, vol. 6, no. 3, pp. 380–384, Mar. 2019.

[17] A. Guarino, G. Poberaj, D. Rezzonico, R. Degl'Innocenti, and P. Günter, "Electro-optically tunable microring resonators in lithium niobate," *Nature Photon.*, vol. 1, no. 7, pp. 407–410, Jul. 2007.

[18] M. Zhang, C. Wang, R. Cheng, A. Shams-Ansari, and M. Lončar, "Monolithic ultra-high-Q lithium niobate microring resonator," *Optica*, vol. 4, no. 12, pp. 1536–1537, Dec. 2017.

[19] Z. Chen, Y. Wang, Y. Jiang, R. Kong, and H. Hu, "Grating coupler on single-crystal lithium niobate thin film," *Opt. Mater.*, vol. 72, pp. 136–139, 2017.

[20] J. D. Witmer, J. T. Hill, and A. H. Safavi-Naeini, "Design of nanobeam photonic crystal resonators for a silicon-on-lithium-niobate platform," *Opt. Express*, vol. 24, no. 6, pp. 5876–5885, Mar. 2016.

[21] H. Liang, R. Luo, Y. He, H. Jiang, and Q. Lin, "High-quality lithium niobate photonic crystal nanocavities," *Optica*, vol. 4, no. 10, pp. 1251–1258, Oct. 2017.
[22] J. D. Bull and N. A. F. Jaeger, "Parasitic mode conversion in *Z*-propagating lithium-niobate waveguides," *J. Lightw. Technol.*, vol. 25, no. 1, pp. 387–393, Jan. 2007.
[23] H. Deng, D. O. Yevick, and S. K. Chaudhuri, "Bending characteristics of asymmetric SOI polarization rotators," *IEEE Photon. Technol. Lett.*, vol. 17, no. 10, pp. 2113–2115, Nov. 2005.
[24] A. V. Tsarev, "New compact polarization rotator in anisotropic $LiNbO_3$ graded-index waveguide," *Opt. Express*, vol. 16, no. 3, pp. 1653–1658, Feb. 2008.
[25] D. Dai and J. E. Bowers, "Novel concept for ultracompact polarization splitter-rotator based on silicon nanowires," *Opt. Express*, vol. 19, no. 11, pp. 10 940–10 949, May 2011.
[26] A. Sakai, T. Fukazawa, and T. Baba, "Estimation of polarization crosstalk at a micro-bend in Si-photonic wire waveguide," *J. Lightw. Technol.*, vol. 22, no. 2, pp. 520–525, Feb. 2004.
[27] M. K. Smit, E. C. M. Pennings, and H. Blok, "A normalized approach to the design of low-loss optical waveguide bends," *J. Lightw. Technol.*, vol. 11, no. 11, pp. 1737–1742, Nov. 1993.
[28] M. Bahadori, M. Nikdast, Q. Cheng, and K. Bergman, "Universal design of waveguide bends in silicon-on-insulator photonics platform," *J. Lightw. Technol.*, vol. 37, no. 13, pp. 3044–3054, Jul. 2019.
[29] Y. Fu, T. Ye, W. Tang, and T. Chu, "Efficient adiabatic silicon-on-insulator waveguide taper," *Photon. Res.*, vol. 2, no. 3, pp. A41–A44, Jun. 2014.
[30] A. Milton and W. Burns, "Mode coupling in optical waveguide horns," *IEEE J. Quantum Electron.*, vol. 13, no. 10, pp. 828–835, Oct. 1977.